International Journal of Heat and Mass Transfer 52 (2009) 239–249

Contents lists available at ScienceDirect

International Journal of Heat and Mass Transfer

journal homepage: www.elsevier.com/locate/ijhmt

Two-dimensional Dual-Phase-Lag thermal behavior in single-/multi-layer structures using CESE method ☆

Yin Chou, Ruey-Jen Yang *

Department of Engineering Science, National Cheng Kung University, Tainan 70101, Taiwan

ARTICLE INFO

Article history:
Received 21 November 2007
Received in revised form 27 June 2008
Available online 20 August 2008

Keywords:
Thermal wave
Dual-Phase-Lag (DPL) model
Conservation Element and Solution Element (CESE) method

ABSTRACT

The Space–Time Conservation Element and Solution Element (CESE) method is used to simulate the propagation of Dual-Phase-Lag (DPL) laser-pulsed thermal waves through single-layer and multi-layer 2D structures. Numerical solutions are presented for the temperature distributions induced within a single-layer structure by four non-Fourier propagation modes, namely hyperbolic, wavelike, diffusive and over-diffusive. In addition, the transmission–reflection phenomena induced as the thermal wave propagates through the interface between two layers with dissimilar properties are systematically examined and discussed.

1. Introduction

In ultra-fast heat conduction systems, the orders of magnitude of the time and space dimensions are extremely short, and thus the traditional Fourier conduction law with its implicit assumption of instantaneous thermal propagation is no longer applicable. As a result, a special treatment is required to model the thermal transport phenomena which take place in nano- and micro-scale systems.

Cattaneo [1] and Vernotte [2] proposed a thermal wave model with a single-phase time lag in which the temperature gradient established after a certain elapsed time was given by

$$\vec{q} + \tau_q \frac{\partial \vec{q}}{\partial t} = -k\nabla T, \tag{1}$$

where τ_q denotes the relaxation time required for the thermal physics to take account of the hyperbolic effect within the medium. From Eq. (1), it can be seen that when $\tau_q > 0$, the thermal wave propagates through the medium with a finite speed of $C = \sqrt{\alpha/\tau_q}$, where α is the thermal diffusivity. However, when τ_q approaches zero, the thermal wave has an infinite speed and thus the Single-Phase-Lag (SPL) model reduces to the traditional Fourier model. The literature contains many investigations into SPL thermal waves. For example, Özisik and Vick [3] presented analytical solutions for the hyperbolic heat conduction equation describing the wavelike nature of thermal energy transport in a finite slab containing a volumetric energy source and having insulated boundaries. Gembarovič and Majerni [4] calculated the temperature distribution resulting from the absorption of an instantaneous pulse of heat flux in a finite medium. Numerical methods using the explicit MacCormack's predictor–corrector or Lax–Wendroff methods have been employed in [5,6] to simulate one-temperature hyperbolic heat conduction problems. In more recent studies, Torii and Yang [7] and Lewandowska and Malinowski [8] used a numerical scheme and an analytical approach, respectively, to investigate the propagation of thermal waves in thin films subjected to a symmetrical heating effect on either side. Gembarovic [9] solved the hyperbolic type heat conduction equation using an explicit iterative finite difference algorithm. However, a significant deviation was observed between the numerical solutions for the thermal wave shape and the exact solutions.

In micro-scale conduction systems, thermal transport takes place through phonons, free electrons and photons. As a result, when the size of the physical system reduces to the characteristic size of these media, it is necessary to take account of certain phenomena which are neglected at the micro-scale, including the phonon–electron interactions, phonon scattering, and so forth. To reflect the effects of these phenomena, Tzou [10] proposed the following Dual-Phase-Lag (DPL) model:

$$\vec{q} + \tau_q \frac{\partial \vec{q}}{\partial t} = -k\left(\nabla T + \tau_T \frac{\partial}{\partial t}\nabla T\right), \tag{2}$$

where τ_T and τ_q denote the finite times required for thermal equilibrium to be obtained and for effective collisions to take place between the electrons and the phonons, respectively. Tang and Araki [11] derived an analytical solution for the DPL model using

☆ A proposed paper submitted to the International Journal of Heat and Mass Transfer.

* Corresponding author. Tel.: +886 6 2002724; fax: +886 6 2766549.
E-mail address: rjyang@mail.ncku.edu.tw (R.-J. Yang).

0017-9310/$ - see front matter © 2008 Elsevier Ltd. All rights reserved.
doi:10.1016/j.ijheatmasstransfer.2008.06.025

Nomenclature

B	lag time ratio ($\tau_T/2\tau_q$)
C	speed of thermal wave
C_p	specific heat
G	amplification matrix
I	laser intensity
k	thermal conductivity
L	length of model
t	time
T	temperature
T_0	reference temperature
q	heat flux
Q	dimensionless heat flux
R	ratio of parameters
W	width of the model
V	volume of Euclidean space E_3

Greek symbols

α	thermal conductivity
β	dimensionless time
γ	ratio of ($\Delta\xi/\Delta\eta$)
η	dimensionless space variable in y direction
ρ	density
τ	thermal relaxation time
θ	dimensionless temperature
ξ	dimensionless space variable in x direction

Superscripts

*	expression of variables in SE
n	time level

Subscripts

0	reference parameter
1	layer 1
2	layer 2
ℓ	number of material
m	matrix element
l	end location of film

Green's function and a finite integral transformation technique. Fan and Lu [12] solved the same problem using a hybrid numerical method combining the Laplace transformation technique and the dual reciprocity boundary element method. However, significant errors were observed between the numerical results and the analytical solutions. Chou and Yang [13] applied the 1D Space–Time Conservation Element and Solution Element (CESE) method to study both SPL model and DPL model thermal wave behavior and performed a numerical stability analysis. Excellent numerical solutions were obtained by the CESE method. Han et al. [14] used a finite difference method to investigate the 2D DPL heat conduction characteristics induced in the short-pulse-laser heating of a surface and presented discussions of the lagging thermal behavior.

In the present study, the 2D DPL heat conduction problem is solved using the CESE method. The CESE method was originally developed by Chang [15] in 1995 as a means of solving the Navier–Stokes and Euler equations, and has been successfully applied to the solution of many computational fluid dynamics and aero-acoustic problems [16]. Zhang et al. [17] demonstrated the application of the CESE method to the numerical solution of 2D and 3D unsteady Euler equations using quadrilateral and hexahedral meshes. Furthermore, Shamsul et al. [18] successfully extended the 2D CESE method to solve the shallow water equations including source terms. The basic principle of the CESE method is to ensure local and global flux conservation in the space and time domains. In the CESE method, the independent flow variables and their derivatives are treated as unknowns and are solved simultaneously. Importantly, there is no need to adjust the artificial dissipation effect to match the local solution properties, and hence an uniform solution accuracy is assured. This feature renders the CESE method an ideal solver for wave problems characterized by discontinuous phenomena or sharp gradients, such as combustion systems, shock waves, ZND waves, and so on. Hence, the CESE method provides a suitable approach for simulating the DPL thermal wave problem, especially the sharp characteristics of SPL (when τ_T is equal to zero, the DPL model reduces to the conventional SPL model).

Previous studies using the DPL diffusion model have reported many interesting phenomena regarding the energy transport at the interface between dissimilar materials [19–22]. However, the DPL model introduces additional mixed spatial- and time-derivative terms in both the governing equation and the boundary conditions imposed at the interface makes mathematical difficult. In the current study, a series of simulations are performed using the CESE scheme and the DPL model to investigate the temperature and heat flux distributions induced by a laser-pulsed thermal wave within a finite 2D structure comprising either one or two slab-like elements. The simulations consider four thermal lagging heat conduction modes, namely hyperbolic, wavelike, diffusive and over-diffusive. The simulations also examine the 2D transmission–reflection

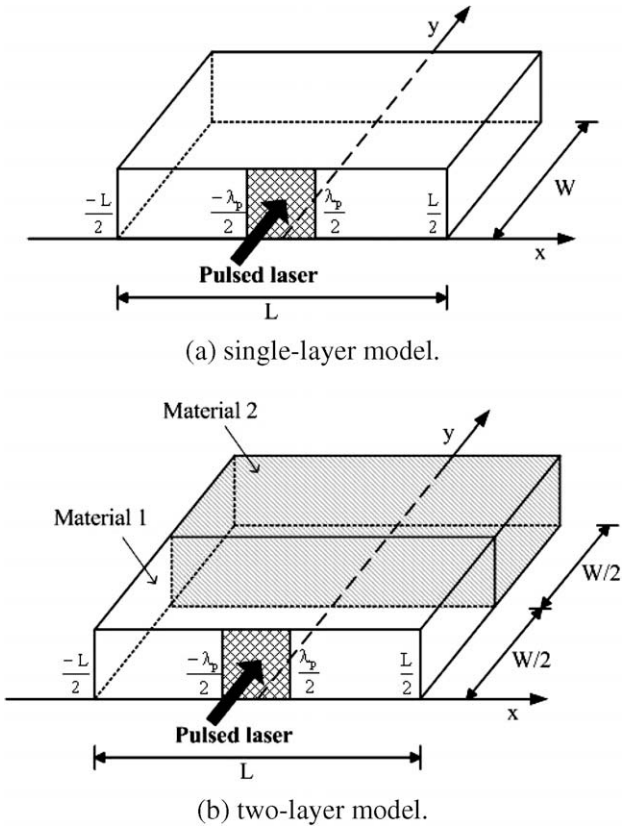

Fig. 1. Simulation models and coordinate system.

phenomenon induced as the thermal energy pulse propagates through the interface between two dissimilar slabs in a two-layered structure.

2. Mathematical models

The current simulations investigate the 2D DPL thermal response of a flat slab subjected to a laser-induced thermal pulse. As shown in Fig. 1(a) and (b), respectively, the simulations consider both a single-layer structure and a two-layer structure comprising slabs of different materials. For simplicity, it is assumed that each medium in the simulation model has a uniform initial temperature, constant thermal properties, and insulated surfaces. Furthermore, in the two-layer model, a perfect connection is assumed between the two slabs (i.e., the thermal resistance of connection on interface is neglected).

The single-layer model is simply a particular case of the two-layer model. Hence, having derived the governing equation for the two-layer model, the corresponding equation for the single-layer model is easily obtained by specifying appropriate parameter values. For the two-layer structure, the DPL model in the x- and y-directions and the energy equation are given, respectively, by

For the 1st material:

$$q_{x1}(x,y,t)+\tau_{q1}\frac{\partial q_{x1}(x,y,t)}{\partial t}=-k_1\left[\frac{\partial T_1(x,y,t)}{\partial x}+\tau_{T1}\frac{\partial}{\partial t}\left(\frac{\partial T_1(x,y,t)}{\partial x}\right)\right], \tag{3}$$

$$q_{y1}(x,y,t)+\tau_{q1}\frac{\partial q_{y1}(x,y,t)}{\partial t}=-k_1\left[\frac{\partial T_1(x,y,t)}{\partial y}+\tau_{T1}\frac{\partial}{\partial t}\left(\frac{\partial T_1(x,y,t)}{\partial y}\right)\right], \tag{4}$$

$$-\left(\frac{\partial q_{x1}(x,y,t)}{\partial x}+\frac{\partial q_{y1}(x,y,t)}{\partial y}\right)=\rho_1 C_{p1}\frac{\partial T_1(x,y,t)}{\partial t}. \tag{5}$$

For the 2nd material:

$$q_{x2}(x,y,t)+\tau_{q2}\frac{\partial q_{x2}(x,y,t)}{\partial t}=-k_2\left[\frac{\partial T_2(x,y,t)}{\partial x}+\tau_{T2}\frac{\partial}{\partial t}\left(\frac{\partial T_2(x,y,t)}{\partial x}\right)\right], \tag{6}$$

$$q_{y2}(x,y,t)+\tau_{q2}\frac{\partial q_{y2}(x,y,t)}{\partial t}=-k_2\left[\frac{\partial T_2(x,y,t)}{\partial y}+\tau_{T2}\frac{\partial}{\partial t}\left(\frac{\partial T_2(x,y,t)}{\partial y}\right)\right], \tag{7}$$

$$-\left(\frac{\partial q_{x2}(x,y,t)}{\partial x}+\frac{\partial q_{y2}(x,y,t)}{\partial y}\right)=\rho_2 C_{p2}\frac{\partial T_2(x,y,t)}{\partial t}. \tag{8}$$

Collectively, these coupled equations describe the temperature and heat flux distributions in the x- and y-directions. Note that in these equations, τ_q and τ_T denote the phase-lag time of the heat flux vector and the temperature gradient, respectively; k is the thermal conductivity of the propagation medium; and C_p is the volumetric heat capacity of the medium.

In the simulations, an assumption is made that the central region of the front surface of the first slab in the two-layer model is irradiated by a laser pulse with a Gaussian distribution in both the temporal and spatial domains, i.e.,

$$I(x,t)=\frac{I_0}{\sqrt{\pi}t_p}\exp\left[-\left(\frac{t}{t_p}\right)^2-\left(\frac{x}{\lambda_p}\right)^2\right], \tag{9}$$

where t_p is the characteristic time in the temporal domain, λ_p is the characteristic length in the spatial domain, and I is the output intensity of the laser.

The present study applies the above physical model to investigate how the thermo-physical property ratios affect the thermo-behavior. For analytical convenience, the following dimensionless variables are introduced for the temperature, heat flux, time and space:

$$\begin{aligned}
&B=\frac{\tau_{T1}}{2\tau_{q1}}, && \xi=\frac{x}{2\sqrt{\alpha_1\tau_{q1}}}, && \eta=\frac{y}{2\sqrt{\alpha_1\tau_{q1}}}, && \beta=\frac{t}{2\tau_{q1}},\\
&\xi_p=\frac{\lambda_p}{2\sqrt{\alpha_1\tau_{q1}}}, && \beta_p=\frac{t_p}{2\tau_{q1}}, && \xi_L=\frac{L}{2\sqrt{\alpha_1\tau_{q1}}}, && \eta_W=\frac{W}{2\sqrt{\alpha_1\tau_{q1}}},\\
&\theta=\frac{\lambda_1\sqrt{\tau_{q1}}\sqrt{\pi}(T-T_0)}{I_0\sqrt{\alpha_1}}, && Q_\xi=\frac{\sqrt{\pi}\tau_{q1}q_{x1}}{I_0}, && Q_\eta=\frac{\sqrt{\pi}\tau_{q1}q_{y1}}{I_0}, && Q_I=\frac{\sqrt{\pi}\tau_{q1}I}{I_0},\\
&R_q=\frac{\tau_{q2}}{\tau_{q1}}, && R_k=\frac{k_2}{k_1}, && R_T=\frac{\tau_{T2}}{\tau_{T1}}, && R_a=\frac{\alpha_2}{\alpha_1},
\end{aligned} \tag{10}$$

where $\alpha = k/\rho C$ is the thermal diffusivity of the propagation medium and B is a dimensionless parameter which characterizes the lagging response and is defined as the ratio between the two phase lags of the 1st material (i.e., $B = \tau_T/2\tau_q$). The properties of the two materials in the two-layer structure, i.e., the lag duration of heat flux, the thermal conductivity, the lag duration of temperature gradient and the thermal diffusivity, can be conveniently defined through an appropriate control of the ratios R_q, R_k, R_T and R_a.

Utilizing these dimensionless variables, the following dimensionless equations can be obtained for the heat flux and temperature distributions in the two slabs within the two-layer structure:

In the 1st slab:

$$\frac{\partial Q_{\xi 1}}{\partial\beta}+\frac{\partial}{\partial\xi}\left(\theta_1+B\frac{\partial\theta_1}{\partial\beta}\right)=-2Q_{\xi 1}, \tag{11}$$

$$\frac{\partial Q_{\eta 1}}{\partial\beta}+\frac{\partial}{\partial\eta}\left(\theta_1+B\frac{\partial\theta_1}{\partial\beta}\right)=-2Q_{\eta 1}, \tag{12}$$

$$\frac{\partial\theta_1}{\partial\beta}+\frac{\partial Q_{\xi 1}}{\partial\xi}+\frac{\partial Q_{\eta 1}}{\partial\eta}=0. \tag{13}$$

In the 2nd slab:

$$R_q\frac{\partial Q_{\xi 2}}{\partial\beta}+R_k\frac{\partial}{\partial\xi}\left(\theta_2+\mathrm{BR}_T\frac{\partial\theta_2}{\partial\beta}\right)=-2Q_{\xi 2}, \tag{14}$$

$$R_q\frac{\partial Q_{\eta 2}}{\partial\beta}+R_k\frac{\partial}{\partial\eta}\left(\theta_2+\mathrm{BR}_T\frac{\partial\theta_2}{\partial\beta}\right)=-2Q_{\eta 2}, \tag{15}$$

$$\frac{R_k}{R_a}\frac{\partial\theta_2}{\partial\beta}+\frac{\partial Q_{\xi 2}}{\partial\xi}+\frac{\partial Q_{\eta 2}}{\partial\eta}=0. \tag{16}$$

Meanwhile, the dimensionless laser irradiation is given by

$$Q_I(\xi,\beta)=\frac{1}{2\beta_p}\exp\left[-\left(\frac{\beta}{\beta_p}\right)^2-\left(\frac{\xi}{\xi_p}\right)^2\right]. \tag{17}$$

Eqs. (11)–(17) represent the governing equations of the two-layer heating model (see Fig. 1(b)). Note that when the properties of 2nd slab are equal to 1st slab, the governing equations will be reduced to single-layer model. Hence, the governing equations for the single-layer model (see Fig. 1(a)) are derived simply by setting the dimensionless ratios R_q, R_k, R_T and R_a equal to 1.

3. Description of CESE scheme

Traditional numerical methods such as finite difference or finite element schemes generally solve the hyperbolic non-Fourier conduction equation for temperature and heat flux separately. However, in this study, the DPL model and associated energy equation are solved at the same time using the CESE scheme. In the current problem, the temperature and the heat flux are both unknowns. Hence, the CESE method is used to derive the solutions of both the temperature and the heat flux simultaneously at each time step.

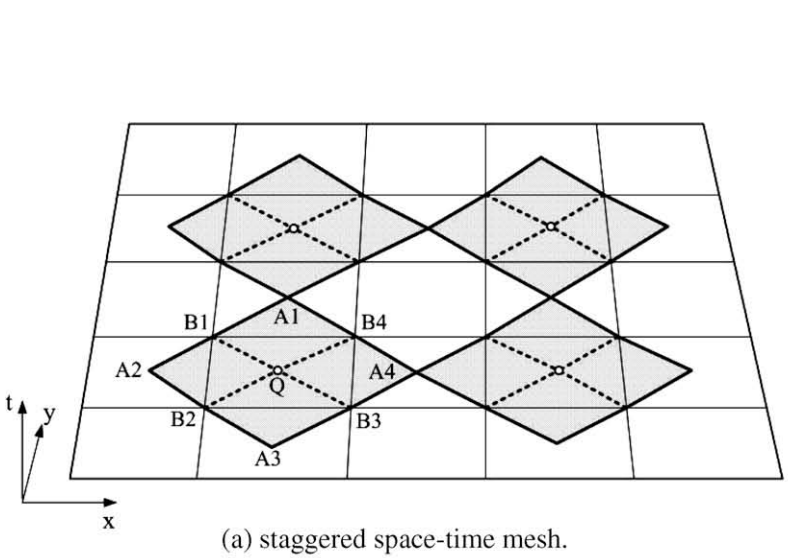

(a) staggered space-time mesh.

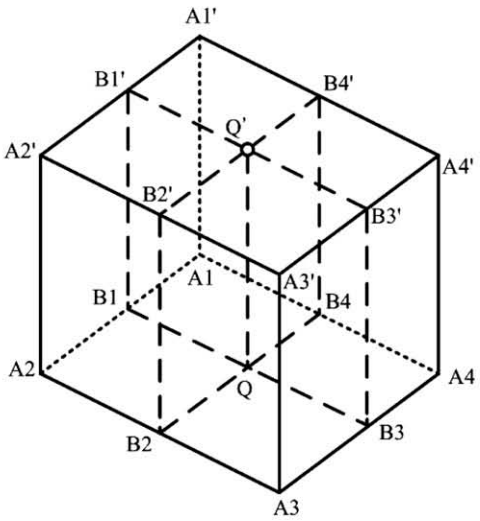

(c) conservation element (CE) of point Q(i,j,n).

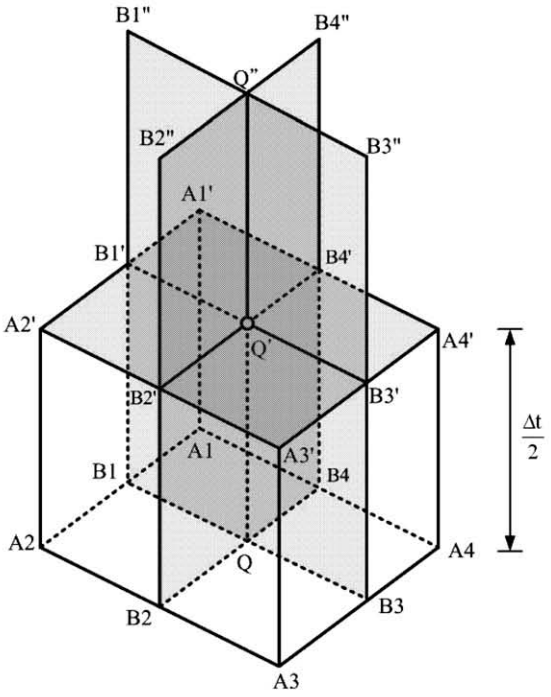

(b) combined conservation element (CE) and solution element at point Q(i,j,n).

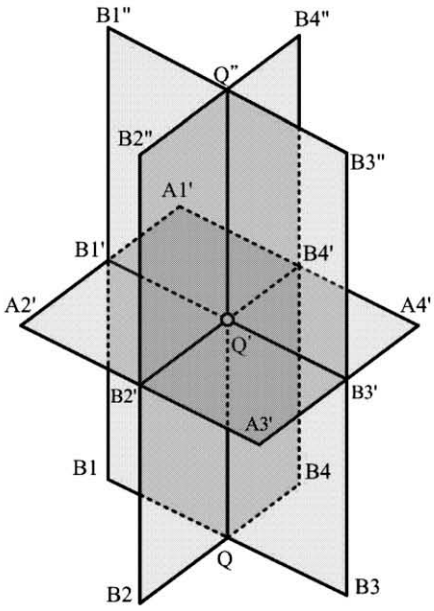

(d) solution element (SE) of point Q(i,j,n).

Fig. 2. Schematic illustration of space–time mesh and elements in CESE scheme.

Table 1
Nodes constituting the four BCEs in CE (Q')

Four BCEs of CE(Q')	
BCE 1	*B4-A1-B1-Q- B4′-A1′-B1′-Q′*
BCE 2	*B1-A2-B2-Q- B1′-A2′-B2′-Q′*
BCE 3	*B2-A3-B3-Q- B2′-A3′-B3′-Q′*
BCE 4	*B3-A4-B4-Q- B3′-A4′-B4′-Q′*

Table 2
Nodes constituting the five faces of SE (Q')

Five faces of SE(Q')	
Face 1	*A1′-B1′-A2′-B2′-A3′ -B3′-A4′-B4′*
Face 2	*B1-B1″-Q″-Q*
Face 3	*B2-B2″-Q″-Q*
Face 4	*B3-B3″-Q″-Q*
Face 5	*B4-B4″-Q″-Q*

The analysis commences by formulating the CESE algorithm for the DPL thermal wave model and the associated energy equation. For simplicity, Eqs. (11)–(16) can be expressed in the following matrix form:

$$\frac{\partial U_{m,\ell}}{\partial \beta}+\frac{\partial F_{m,\ell}}{\partial \xi}+\frac{\partial G_{m,\ell}}{\partial \eta}=S_{m,\ell},\quad m=1,2,3 \text{ and } \ell=1,2. \tag{18}$$

where the "m" indicates the number of variables and "ℓ" denotes the number of different materials in the heat model (i.e., one or

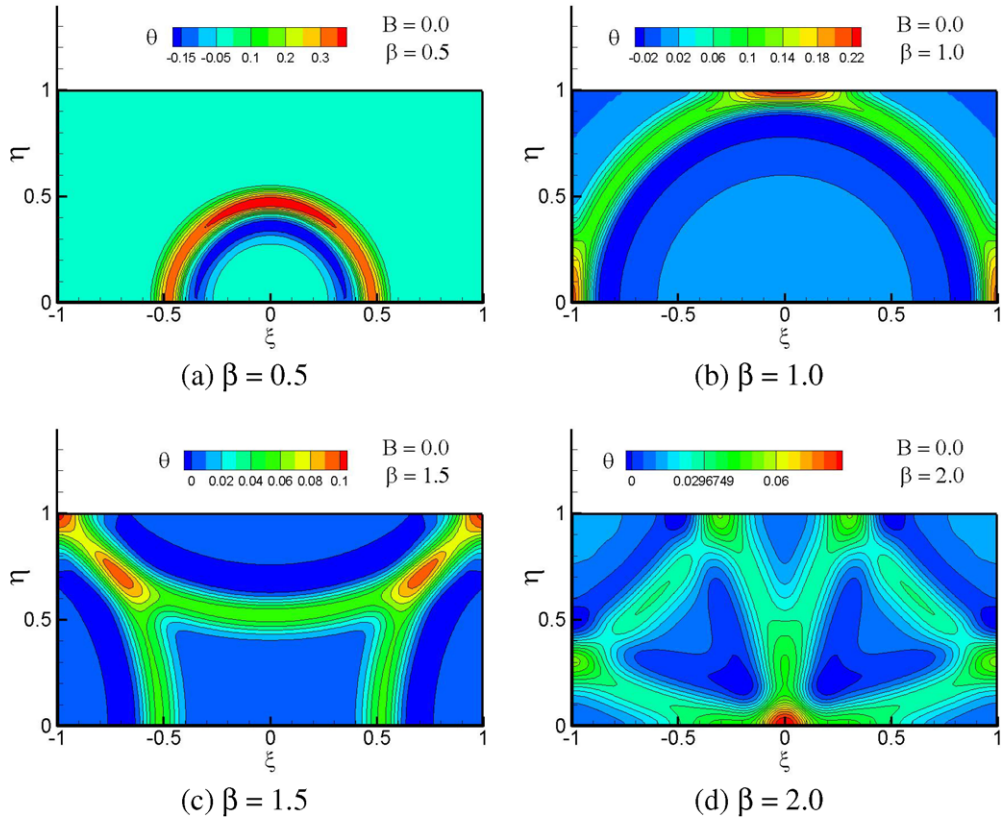

Fig. 3. Transient temperature distribution associated with hyperbolic wave behavior at $B = 0.0$.

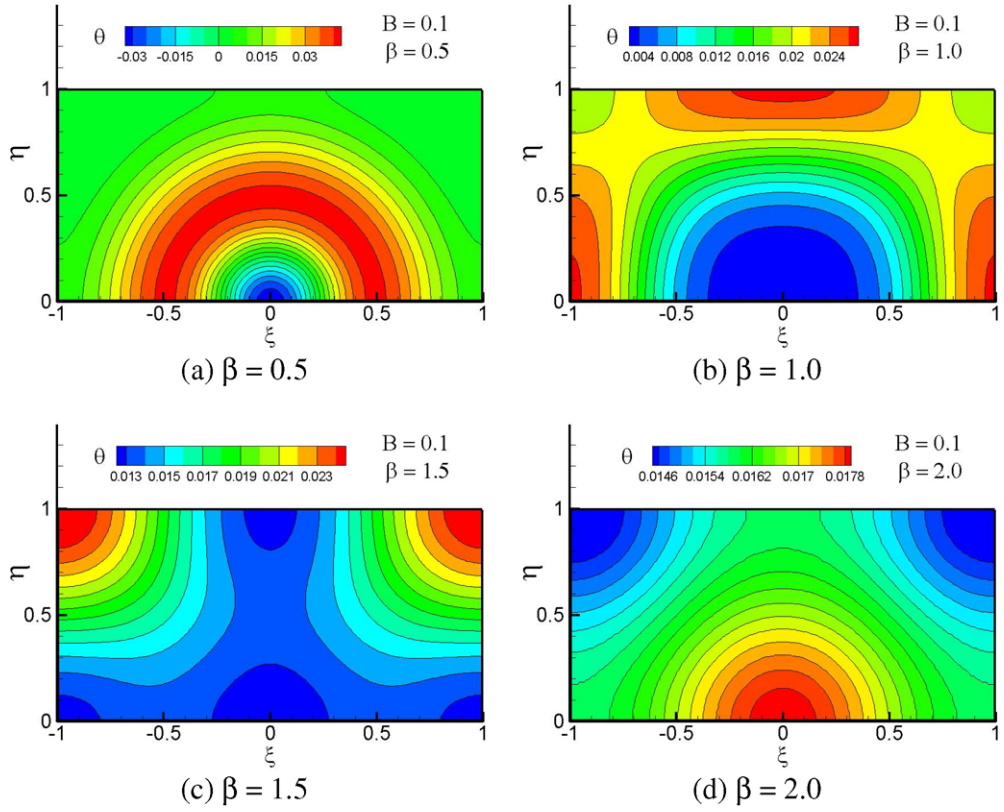

Fig. 4. Transient temperature distribution associated with wavelike behavior at $B = 0.1$.

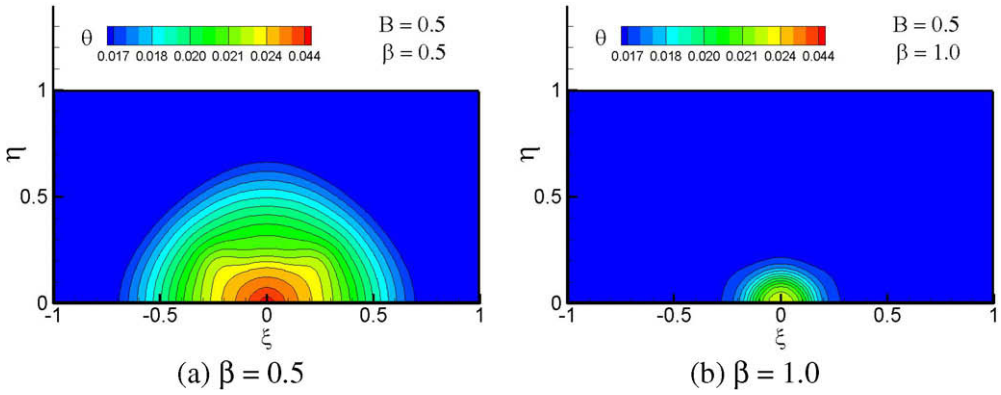

Fig. 5. Transient temperature distribution associated with diffusive behavior at $B = 0.5$.

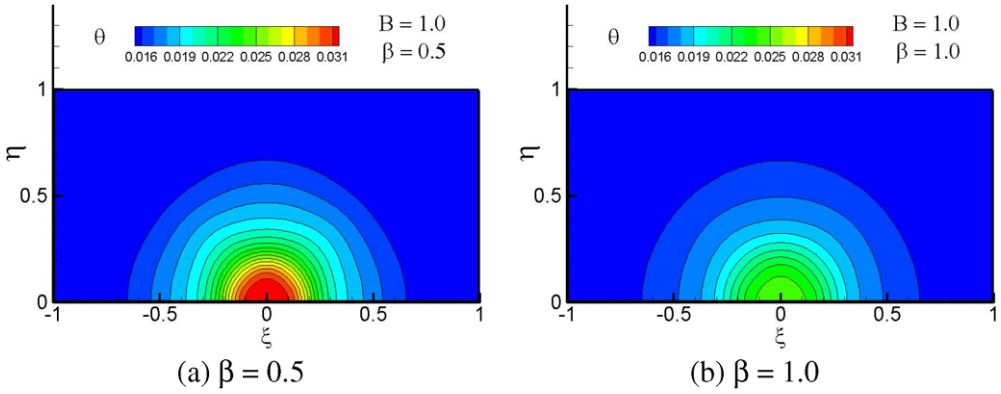

Fig. 6. Transient temperature distribution associated with over-diffusive behavior at $B = 1.0$.

two in the current case). The various components of this matrix are defined as follows:

$$U_{m,1}=\begin{bmatrix}Q_{\xi 1}\\ Q_{\eta 1}\\ \theta_1\end{bmatrix},\quad F_{m,1}=\begin{bmatrix}\theta_1+B\theta_{\beta 1}\\ 0\\ Q_{\xi 1}\end{bmatrix},\quad G_{m,1}=\begin{bmatrix}0\\ \theta_1+B\theta_{\beta 1}\\ Q_{\eta 1}\end{bmatrix},$$

$$S_{m,1}=\begin{bmatrix}-2Q_{\xi 1}\\ -2Q_{\eta 1}\\ 0\end{bmatrix},$$

$$U_{m,2}=\begin{bmatrix}Q_{\xi 2}\\ Q_{\eta 2}\\ \theta_2\end{bmatrix},\quad F_{m,2}=\begin{bmatrix}\frac{R_k}{R_q}(\theta_2+\mathrm{BR}_T\theta_{\beta 2})\\ 0\\ (R_aQ_{\xi 2})/R_k\end{bmatrix},\quad G_{m,2}=\begin{bmatrix}0\\ \frac{R_k}{R_q}(\theta_2+\mathrm{BR}_T\theta_{\beta 2})\\ (R_aQ_{\eta 2})/R_k\end{bmatrix},$$

$$S_{m,2}=\begin{bmatrix}-2Q_{\xi 2}/R_q\\ -2Q_{\eta 2}/R_q\\ 0\end{bmatrix}.$$

Let $x_1 = \xi$, $x_2 = \eta$ and $x_3 = \beta$ be the coordinates of a 3D Euclidean space, E_3. Applying the Gaussian divergence theorem within E_3, the differential form of Eq. (18) can be transformed into the following integral conservation form:

$$\oint_{S(V)}\vec{h}_m\cdot d\vec{s}=\int_V (F_m)dV,\quad m=1,2,3, \tag{19}$$

where $\vec{h}_m=(F_m,G_m,U_m)$, and $S(V)$ is the boundary of an arbitrary space–time region V within E_3. Essentially, the right hand side of Eq. (19) is a volume integration representing the internal heat generated over region V.

As shown in Fig. 2(a), the Euclidean space, E_3, is divided into an array of non-overlapping octagonal cylindrical regions referred to as conservation elements (CEs). Fig. 2(b) shows the combined CE and solution element (SE) associated with point $Q(i,j,n)$. The face of octagon $A1$, $B1$, $A2$, $B2$, $A3$, $B3$, $A4$, $B4$, whose centroid is denoted as $Q(i,j,n)$. Furthermore, point Q is assigned as solution point. Similarly, $A1$, $A2$, $A3$, $A4$ is refer to another's centroid of octagon, respectively. Fig. 2(c) illustrates the structure of the CE associated with point $Q(i,j,n)$. In practice, every CE is formed by four basic conservation elements (BCEs) each with the shape of a quadrilateral cylinder (see Table 1). Finally, Fig. 2(d) presents a schematic illustration of the SE. As shown, the SE comprises five faces (see Table 2).

For any $(\xi,\eta,\beta)\in SE(i,j,n)$, assuming a linear distribution in the SE, the values of U_m^*, F_m^*, G_m^* and $\vec{h}_m^*$ at any position in the SE can be approximated by U_m, F_m, G_m and $\vec{h}_m$ at point (i,j,n), respectively. The first-order Taylor's expansions of U_m, F_m and G_m are given, respectively, by

$$\begin{aligned}
U_m^*|_{i,j,n}^{\xi,\eta,\beta}&=(U_m)_{i,j}^n+(\xi-\xi^n)(U_{m\xi})_{i,j}^n+(\eta-\eta_j)(U_{m\eta})_{i,j}^n+(\beta-\beta_j)(U_{m\beta})_{i,j}^n,\\
F_m^*|_{i,j,n}^{\xi,\eta,\beta}&=(F_m)_{i,j}^n+(\xi-\xi^n)(F_{m\xi})_{i,j}^n+(\eta-\eta_j)(F_{m\eta})_{i,j}^n+(\beta-\beta^j)(F_{m\beta})_{i,j}^n,\\
G_m^*|_{i,j,n}^{\xi,\eta,\beta}&=(G_m)_{i,j}^n+(\xi-\xi^n)(G_{m\xi})_{i,j}^n+(\eta-\eta_j)(G_{m\eta})_{i,j}^n+(\beta-\beta^j)(G_{m\beta})_{i,j}^n,\\
&m=1,2,3.
\end{aligned} \tag{20}$$

Meanwhile, $\vec{h}_m\equiv(F_m,G_m,U_m)$, for any $m = 1, 2, 3$, can be approximated by

$$\vec{h}_m^*|_{i,j,n}^{\xi,\eta,\beta}=(U_m^*(\xi,\eta,\beta;i,j,n),F_m^*(\xi,\eta,\beta;i,j,n),G_m^*(\xi,\eta,\beta;i,j,n)). \tag{21}$$

In Eq. (20), $U_m^*|_{i,j,n}^{\xi,\eta,\beta}$ describes the extension of U_m^* from node (i,j,n) to (ξ,η,β). Similarly, $F_m^*|_{i,j,n}^{\xi,\eta,\beta}$, $G_m^*|_{i,j,n}^{\xi,\eta,\beta}$, and $h_m^*|_{i,j,n}^{\xi,\eta,\beta}$ describe the extensions of F_m^*, G_m^* and $\vec{h}_m^*$, respectively, from node (i,j,n) to (ξ,η,β). Note that

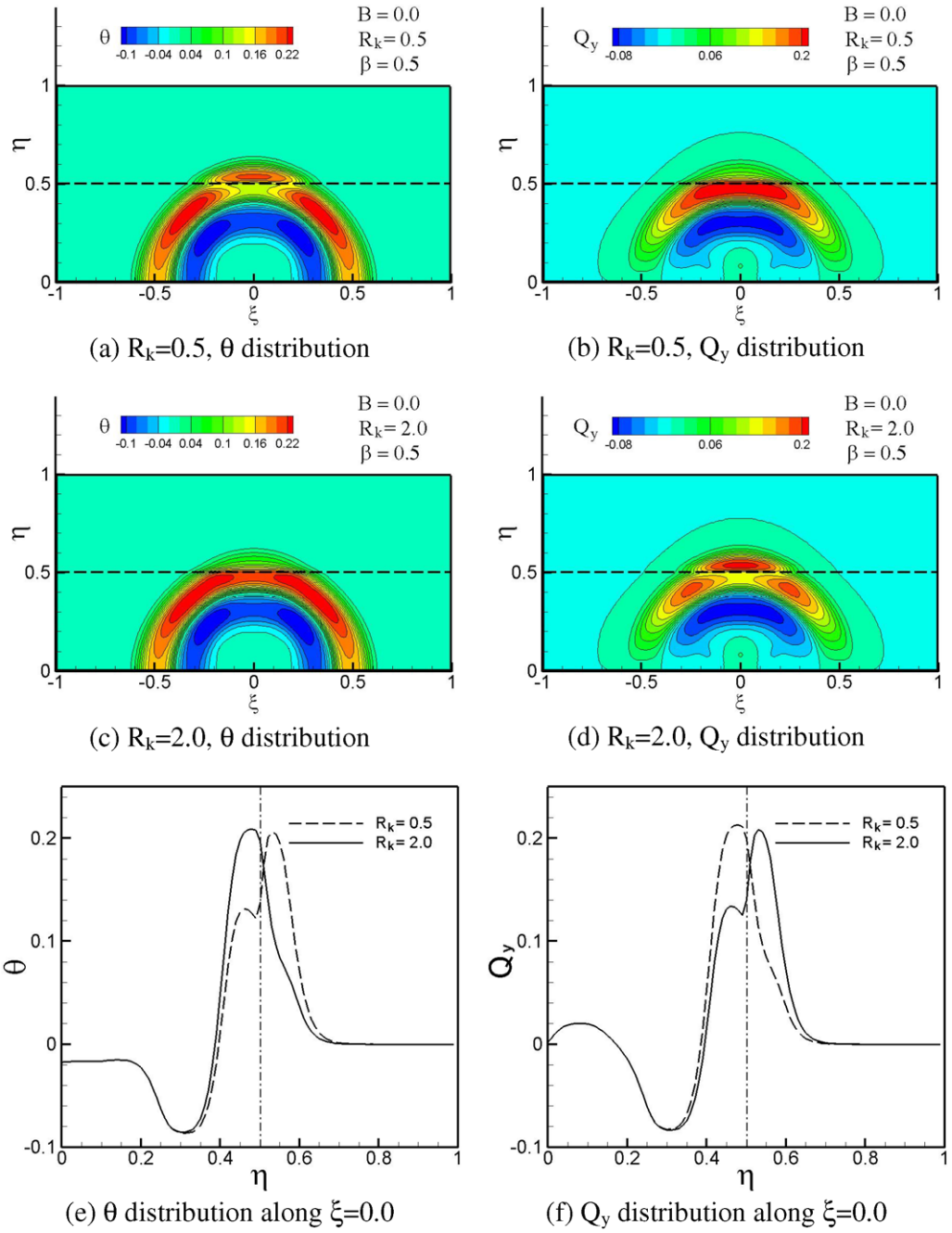

Fig. 7. Effect of R_k on θ and Q_y at $\beta = 0.5$ as wave propagates through two-layer structure with $B = 0.0$.

in every case, the subscript (i,j) is the node index of A1, A2, A3 or A4 in Fig. 2(a). The partial derivatives of F and G can be related to that of U by applying the chain rule with the value of U_β provided by Eq. (18). The surface flux can be easily calculated by evaluating the flux vectors at the geometrical center of the surface using the Taylor's series expansions.

At some time level n, the solution procedure yields the variables U, U_x and U_y at the four nodes A1, A2, A3 and A4 in Fig. 2(b), and the aim is to compute U, U_x and U_y at O' at the next time level $(n + 1/2)$. To do so, Eq. (19) is applied to each of the four BCEs, and enforce the conservation of the total flux of h^*_m leaving the conservation element of Q' through its surface and the quantities generated by volume integration of source term F_m. Detail procedures to treat the source term with the CESE scheme can be found in [18]. Hence, the unknown value of U_m at O' can be found. Having derived U_m, the unknowns U_{mx} and U_{my} can be computed based on the weighting skills, as described in [17].

4. Results and discussion

Numerical simulations were performed to investigate the 2D lagging thermal conduction behavior induced in a single-layer structure by a short laser pulse with both temporal and spatial dimensions. The temperature distributions obtained using the hyperbolic, wavelike, diffusive and over-diffusive non-Fourier thermal propagation models are presented in Figs. 3–6, respectively. The numerical results obtained for the temperature and heat flux distributions as the thermal disturbance propagates through the interface of the two-layer structure are presented in Figs. 7–10. Note that in all cases, the simulations involve a total of 20,000 cells.

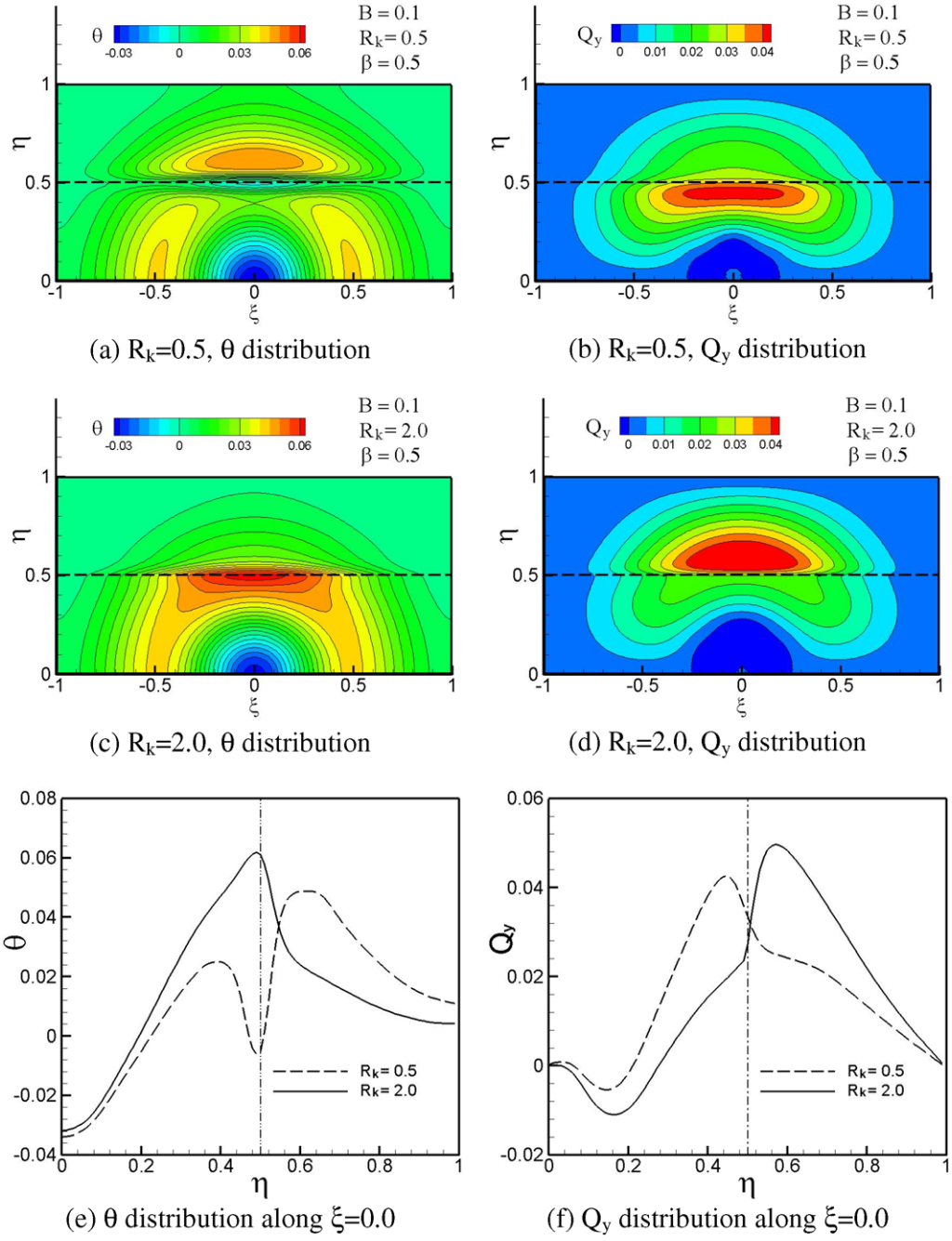

Fig. 8. Effect of R_k on θ and Q_y at $\beta = 0.5$ as wave propagates through two-layer structure with $B = 0.1$.

Figs. 3–6 show the evolution of the temperature distribution in a single-layer structure of length $\xi_L = 2$ and thickness $\xi_W = 1$ irradiated by a laser pulse with a characteristic time of $\beta_p = 0.1$ and a characteristic length of $\xi_p = 0.1$. Note that the time increment is 5×10^{-4}. In general, the lag time ratio, B, controls the transition between the various thermal conductions modes, i.e., hyperbolic, wavelike, diffusive, and over-diffusive. Fig. 3 illustrates the evolution of the temperature distribution for the case of $B = 0$, i.e., $\tau_T = 0$. As shown, under these conditions, the pulsed thermal disturbance propagates in the form of a hyperbolic wave. It can be seen that the wave propagates throughout the slab (i.e., $\beta = 0.5$ and $\beta = 1.0$), strikes the rear and side surfaces of the slab and is reflected ($\beta = 1.5$), and then forms a superimposed structure comprising the waves reflected from the various slab surfaces ($\beta = 1.5$ and $\beta = 2.0$). These results also show good agreements with those in reference [14].

Fig. 4 considers the case where B is increased to a value of 0.1. In this case, the pulsed thermal disturbance is dissipated by the diffusive effect of τ_T. In general, for all values of the lag time ratio in the range $0 \leqq B < 0.5$, i.e., $\tau_T < \tau_q$, wave features such as propagation and reflection can be observed. However, a hyperbolic wave behavior occurs only when B is equal to zero. Strictly speaking, the temperature response in the range $0 < B < 0.5$ exhibits a wavelike behavior. Observing Figs. 3 and 4, it can be seen that the hyperbolic wave behavior and the wavelike behavior both result in the formation of local temperature peaks within the slab due to the superimposition of the thermal waves reflected from the various surfaces of the slab.

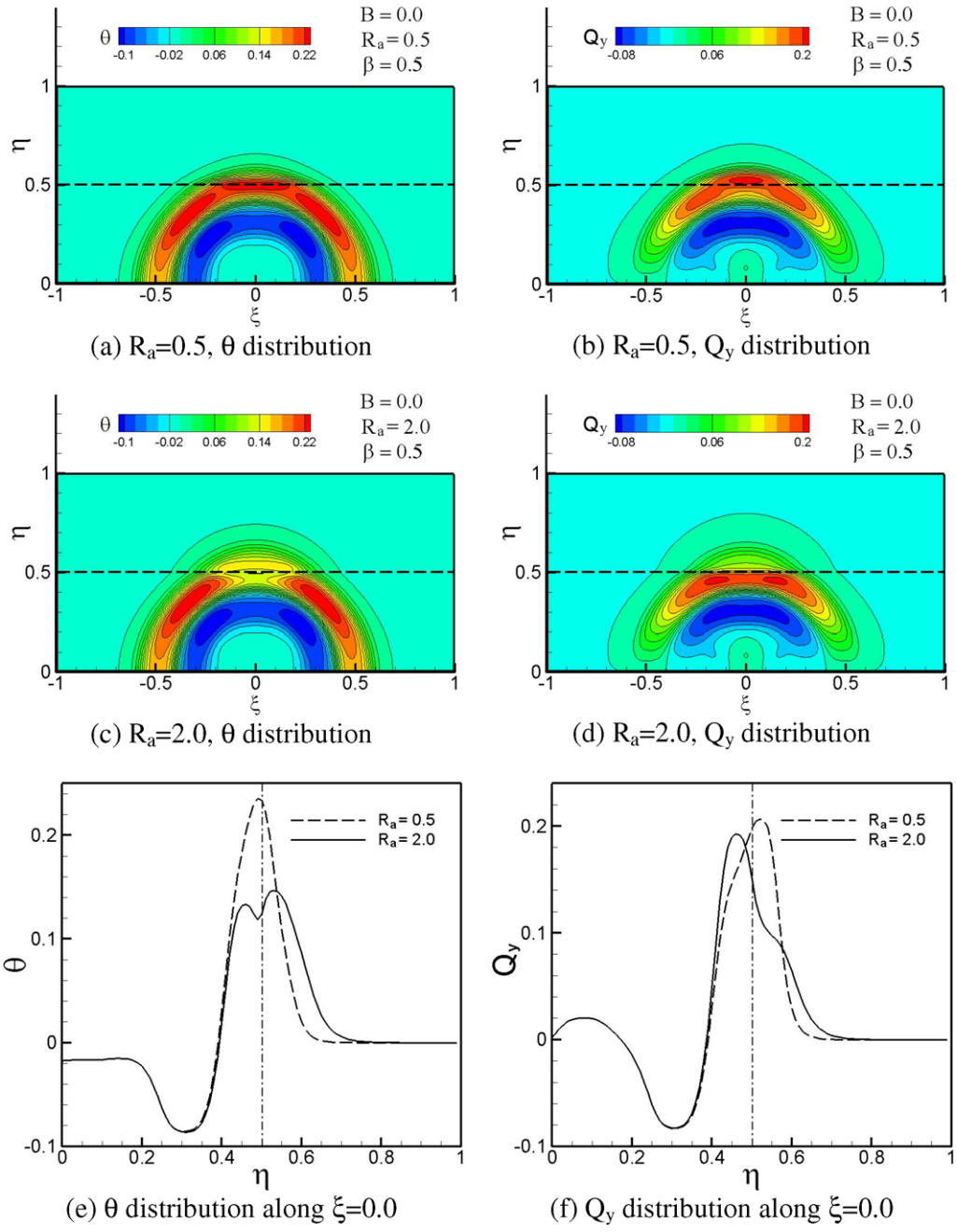

Fig. 9. Effect of R_a on θ and Q_y at $\beta = 0.5$ as wave propagates through two-layer structure with $B = 0.0$.

When the lag time ratio is further increased to $B = 0.5$, Fig. 5 shows that all of the wave and wavelike features disappear and are replaced by a diffusive type transport mechanism. Under these conditions, the peak temperature occurs in the region of the slab at which the laser pulse is applied. Fig. 6 shows the case where the lag time ratio is increased to $B = 1.0$. In this case, $\tau_T > \tau_q$ and it can be seen that an over-diffusive behavior is induced. Comparing Figs. 5 and 6, it is observed that a larger value of τ_T enhances the thermal diffusion effect and therefore prompts a more rapid temperature response in the period immediately following the application of the thermal pulse. However, a longer period of time is required for the thermal distribution to reach equilibrium conditions than that required in the classical diffusion case.

Figs. 7–10 illustrate the hyperbolic and wavelike propagation of the pulsed thermal disturbance through a two-layer structure. Due to the nature of the CESE scheme, no solution point exists on the interface boundary, and thus the problem of uncertainties at the interface between the two dissimilar materials in the two-layer structure is avoided. The flux conservation concept inherent in the CESE method enables clear insights to be obtained into the behavior of the thermal wave as it propagates through the interface separating the two dissimilar slabs. Fig. 7 illustrates the effect of parameter R_k on the propagation of the thermal wave at $\beta = 0.5$ for conditions of $B = 0.0$ and $R_T = R_q = R_a = 1$. Since B has a value of zero, the thermal disturbance exhibits a hyperbolic propagation mode. A prominent reflection-transmission phenomenon can be observed at the interface of the two slabs. At the elapsed time considered in this figure ($\beta = 0.5$), the thermal wave front has encountered the interface and thus the temperature and heat flux distributions are both dependent on the thermal properties of

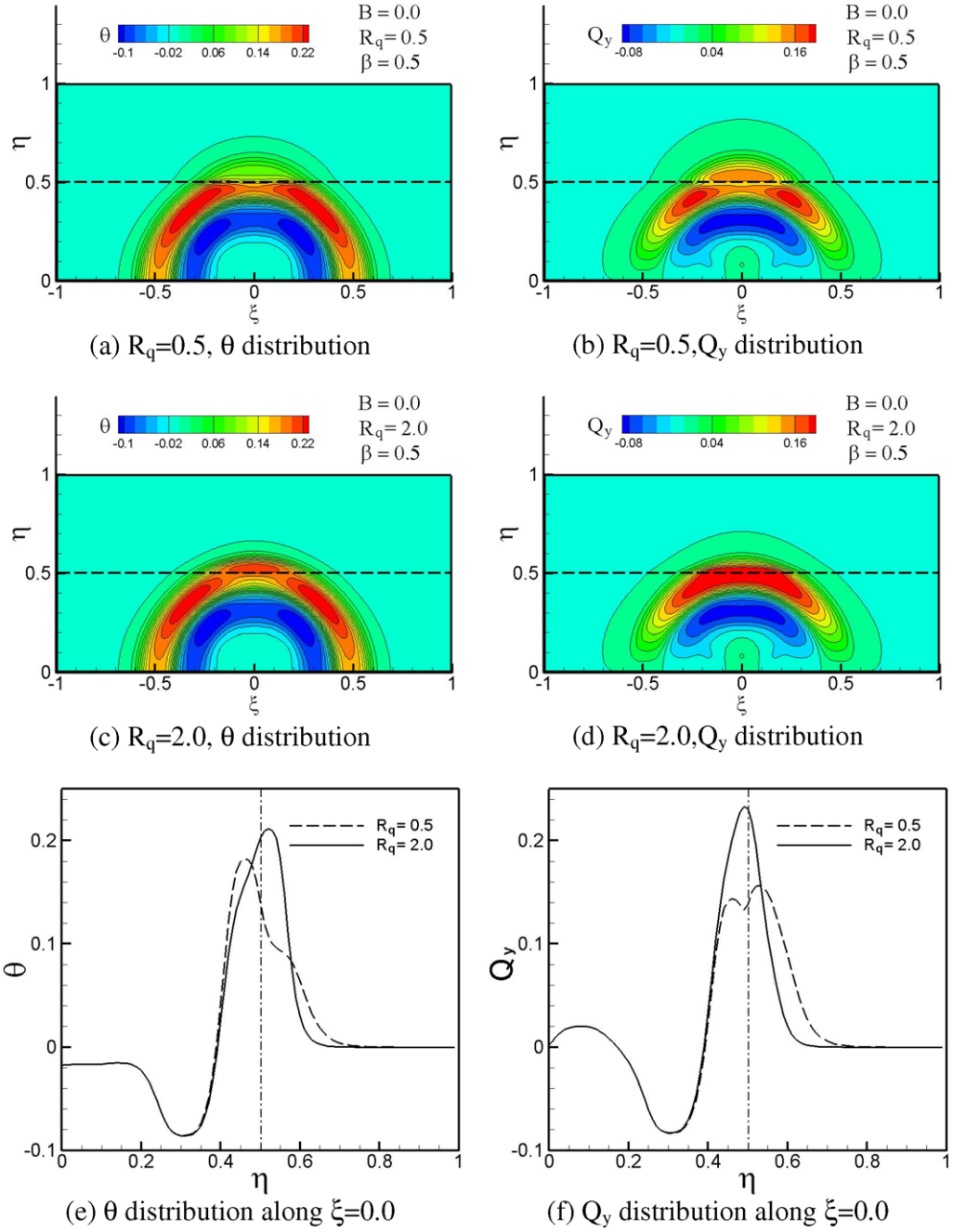

Fig. 10. Effect of R_q on θ and Q_y at $\beta = 0.5$ as wave propagates through two-layer structure with $B = 0.0$.

the second slab in the two-layer structure. For the case where the second layer has a higher thermal conductivity (i.e., $R_k = 2.0$), the slab has a greater ability to transmit the thermal energy when the wave front impacts the interface. Therefore, the heat flux in the second layer increases as the value of R_k increases (Fig. 7(f)), thus causing a reduction of temperature distribution near the interface in 1st slab (Fig. 7(e)). However, it can be seen that the locations of the thermal wave fronts in Fig. 7(e) and (f) remain unchanged as R_k is increased from 0.5 to 2.0. As a result, it can be inferred that the propagation velocity of the thermal wave is independent of the thermal conductivity of the two media in the two-layer structure. Fig. 8 illustrates the results obtained for the propagation of the thermal wave at time $\beta = 0.5$ under conditions of $B = 0.1$ and $R_k = 0.5$ or 2.0. Similar trends are observed to those presented in Fig. 7. However, in this case, the pulsed thermal disturbance is dissipated by the diffusive effect of τ_T, resulting in a wavelike propagation behavior.

Fig. 9 shows the effect of R_a on the temperature and heat flux distributions in the two-layer structure under conditions of $B = 0.0$ and $\beta = 0.5$. The thermal wave propagates through the first and second layers of the structure at velocities of $C_1 = \sqrt{\alpha_1/\tau_{q1}}$ and $C_2 = \sqrt{\alpha_2/\tau_{q2}}$, respectively. From the definition above, the ratio of C_2 to C_1 can be written as $C_2 = C_1\sqrt{R_a/R_q}$. Thus, in Fig. 9, it can be seen that the propagation speed of the transmitted wave in the second slab increases as the value of R_a increases. By contrast, Fig. 10 shows that the transmitted wave propagates more rapidly in the second layer as the value of R_q decreases.

It is well known that in a medium with a low volumetric heat capacity, ρC_p, the amount of energy absorbed as a thermal wave propagates through it is limited and thus a lower temperature rise

is induced. Hence, a higher value of the thermal diffusivity, α, increases the temperature profile because ρC_p varies inversely with α for a constant thermal conductivity. As a result, an increased value of R_a increases the magnitude of the transmitted wave front in the second slab of the two-structure layer.

5. Conclusion

This study has performed a series of CESE simulations based on the DPL thermal model to investigate the propagation characteristics of a laser-induced thermal disturbance within single- and two-layer structures. By varying the lag time ratio ($B = \tau_{T1} / 2\tau_{q1}$), the simulations have illustrated the evolutions of the temperature and heat flux distributions under various 2D lagging heat conduction mechanisms, namely hyperbolic, wavelike, diffusive and over-diffusive. Furthermore, the complex reflection-transmission phenomena which occur as the thermal disturbance encounters the interface between two dissimilar slabs in a multiple-layer structure have been presented for both the hyperbolic and the wavelike propagation modes. The CESE method resolves the complex thermal wave interactions with excellent accuracy.

References

[1] C. Cattaneo, A form of heat conduction equation which eliminates the paradox of instantaneous propagation, Compute Rendus 247 (1958) 431–D433.
[2] P. Vernotte, Les paradoxes de la theorie continue de l' equation de la chaleur, Compute Rendus 246 (1958) 3145–D3155.
[3] M.N. Özisik, B. Vick, Propagation and reflection of thermal waves in a finite medium, Int. J. Heat Mass Transf. 27 (1984) 1845–1854.
[4] J. Gembarovič, V. Majerni, Non-Fourier propagation of heat pulses in finite medium, Int. J. Heat Mass Transf. 31 (5) (1988) 1073–1080.
[5] D.E. Glass, M.N. Ozisik, D.S. McRae, Hyperbolic heat conduction with radiation in an absorbing and emitting medium, Numer. Heat Transf. 12 (1987) 321–333.
[6] D.E. Glass, M.N. Ozisik, D.S. McRae, B. Vick, On the numerical solution of hyperbolic heat conduction, Numer. Heat Transf. 8 (1985) 497–504.
[7] S. Torii, W.J. Yang, Heat transfer mechanisms in thin film with laser heat source, Int. J. Heat Mass Transf. 48 (2005) 537–544.
[8] M. Lewandowsda, L. Malinowski, An analytical solution of the hyperbolic heat conduction equation for the case of a finite medium symmetrically heated on both sides, Int. Commun. Heat Mass Transf. 33 (2006) 61–69.
[9] J. Gembarovic, Non-Fourier heat conduction modeling in a finite medium, Int. J. Thermophys. 25 (2004) 1261–1268.
[10] D.Y. Tzou, Macro-to microcale heat heat transfer: the lagging behavior, Taylor & Francis, Washington, DC, 1996. pp. 25–29.
[11] D.W. Tang, N. Araki, Non-Fourier heat conduction behavior in finite mediums under pulse surface heating, Mater. Sci. Eng. A292 (2000) 173–178.
[12] Q.M. Fan, W.Q. Lu, A new numerical method to simulate the non-Fourier heat conduction in a single-phase medium, Int. J. Heat Mass Transf. 45 (2002) 2815–2821.
[13] Y. Chou, R.J. Yang, Application of CESE method to simulate non-Fourier heat conduction in finite medium with pulse surface heating, Int. J. Heat Mass Transf. 51 (2008) 3525–3534.
[14] P. Han, D.W. Tang, L.P. Zhou, Numerical analysis of two-dimensional lagging thermal behavior under short-pulse-laser heating on surface, Int. J. Eng. Sci. 44 (2006) 1510–1519.
[15] S.C. Chang, The method of space–time conservation element and solution element – a new approach for solving the Navier–Stokes and Euler equations, J. Comput. Phys. 119 (1995) 295–324.
[16] C.Y. Loh, L.S. Hultgren, S.C. Chang, Wave computation in compressible flow using space–time conservation element and solution element method, AIAA J. 39 (2001) 794–801.
[17] Z.C. Zhang, S.T. John Yu, S.C. Chang, A space–time conservation element and solution element method for solving the two- and three-dimension unsteady euler equations using quadrilateral and hexahedral meshes, J. Comput. Phys. 175 (2002) 168–199.
[18] Q. Shamsul, W. Gerald, Application of space–time CESE method to shallow water magnetohydrodymic equations, J. Comput. Appl. Math. 196 (2006) 132–149.
[19] J.K. Chen, J.E. Beraun, D.Y. Tzou, A Dual-Phase-Lag diffusion model for interfacial layer growth in metal matrix composites, J. Mater. Sci. 34 (1999) 6183–6187.
[20] J.K. Chen, J.E. Beraun, Numerical study of ultrashort laser pulse interactions with metal films, Numer. Heat Transf. A 40 (2001) 1–20.
[21] J.K. Chen, J.E. Beraun, D.Y. Tzou, A Dual-Phase-Lag diffusion model for predicting intermetallic compound layer growth in solder joins, ASME J. Electron. Packaging 123 (2001) 52–57.
[22] K.C. Liu, Analysis of Dual-Phase-Lag thermal behavior in layered films with temperature-dependent interface thermal resistance, J. Phys. D: Appl. Phys. 38 (2005) 3722–3732.